Adsorption (2006) 12:339–360
DOI 10.1007/s10450-006-0564-y

MFI zeolite membranes from *a*- and randomly oriented monolayers

Jungkyu Choi · Shubhajit Ghosh · Lisa King · Michael Tsapatsis

Abstract *c*-Oriented columnar MFI films made by secondary growth of randomly oriented seed monolayers, deposited using sonication-assisted covalent attachment, exhibit *n*-hexane/2,2-dimethylbutane separation factor of up to 10^4, *n*-/*i*-butane separation factor of up to 50, and *p*-/*o*-xylene separation factor of up to 2. A MFI film from *a*-oriented seed layer shows lower separation factors for the linear vs. branched isomers but higher separation factor for *p*-/*o*-xylene.

Keywords Zeolite · MFI · Preferred orientation · Butane · Hexane · Xylene · Permeation · Separation

1 Introduction

This paper is dedicated to the late Dr. John Sherman. John was a pioneer in adsorption, separations and ion exchange. John had an illustrious career reaching Senior Corporate Fellow at Union Carbide Corporation and later at UOP LLC. After retiring from UOP at the end of 1999 he taught at the University of Massachusetts Amherst for several years. He was well known in the scientific community for his work in adsorption. Highlights included the development of Crystalline SilicoTitanates (UOP IE-910 and IE-911) for remediation of radioactive ^{137}Cs from wastewater accumulated at DOE sites across the country. This effort won UOP a "Top 100 Award" from R&D Magazine in 1996. In his personal life, John was a devoted family man who enjoyed sailing in the waters off Cape Cod. He is sorely missed by many.

John had many insights to share with his co-workers and the zeolite community as the development of zeolitic membranes began with earnest in the 1990's. Despite the significant progress in reproducibly controlling microstructure (Jiang et al., 2004) and improving separation performance (Hedlund et al., 2002; Lai et al., 2003), zeolite membrane technology has had limited commercial impact up to now because the reproduction of ultra-thin and defect-free zeolite membranes on a large scale is difficult (McLeary and Jansen, 2004). Although some of the initial worries regarding flux limitations prohibiting commercial use have been addressed (Meindersma and de Haan, 2002), major concerns remain regarding scale up and manufacturing costs (Coronas and Santamaria, 2004; Caro et al., 2005; McLeary et al., 2006).

It is by now well established that it is possible to employ zeolite MFI membranes to separate isomers of hydrocarbons (Lin et al., 2002; Noack et al., 2002). This becomes possible because of the size sensitivity of the zeolite membrane (Davis, 2002) which can differentiate between, for example, linear and branched

J. Choi · S. Ghosh · M. Tsapatsis (✉)
Department of Chemical Engineering and Materials Science, University of Minnesota, 151 Amundson Hall, 421 Washington Ave. SE, Minneapolis, MN 55455, USA
e-mail: tsapatsi@cems.umn.edu

L. King
UOP LLC, 25 E. Algonquin Rd, Des Plaines, IL 60017-5017

isomers, the former being of smaller critical dimension independent of the molecular weight and length. This is unlike other methods, such as fractional distillation, which is sensitive primarily to the molecular weight in a homologous series such as hydrocarbons. Thus while fractional distillation separates the petroleum hydrocarbon mixture mainly according to the molecular weight, the zeolite MFI membrane separates mainly linear from branched hydrocarbons based on the nature of sorption and diffusion along with molecular sieving effect (Caro et al., 2000).

Previous studies indicate that zeolite MFI membrane performance (permeance and separation factor) varies considerably depending on film microstructure. For example, it has been demonstrated that thick columnar *c*-oriented zeolite films are highly selective for *n*-/*i*-butane, while they exhibit very low, if any, *p*-/*o*-xylene separation factors (Xomeritakis et al., 1999, 2000, 2001). On the other hand, thin *h0h*-oriented and thin random and *b*-oriented films exhibit the reverse trend, i.e., increasingly more selective for *p*-/*o*-xylene and less selective for *n*-/*i*-butane (Xomeritakis et al., 2001; Hedlund et al., 2002, 2003; Lai et al., 2003; Lai and Tsapatsis, 2004).

Factors contributing to these differences include MFI channel orientation (Lai et al., 2003), grain boundary structure (Bonilla et al., 2001; Bons and Bons, 2003), defects like cracks and pinholes (Xomeritakis et al., 1999) and possibly strain induced diffusivity and adsorption changes (Jeong et al., 2005).

In this report we present information regarding the microstructure and permeation performance of membranes prepared using *a*-oriented seed layers (Choi et al., 2006) and compare with membranes made from randomly oriented ones. Some of the seed monolayers are deposited with a recently introduced fast deposition technique under sonication (Lee et al., 2005) that is promising with respect to scale-up.

2 Experimental

2.1 Support

The fabrication process of MFI membranes is presented in Scheme 1 (see also (Mabande et al., 2005). 2 mm-thick α-alumina discs, 22 mm in diameter, were made by pressing (Carver) alumina power (Baikowski International Corp., CR6 grade). The discs were sintered at 800°C for 30 h with 1°C/min followed by heating up to 1180°C for 12 h. Heating rate was controlled to 1°C/min. One side of the discs was polished (grit 600). After drying in an oven overnight, surfactant-templated aged silica sol was coated on the polished side of discs by contacting the polished side with the sol for 20 sec and allowing for solvent evaporating for 40 sec while the discs were held vertically. Subsequently, surfactant was removed by calcination (480°C for 4 h with 1°C/min ramp rate under 150 ml/min air flow).

Silica sol was prepared based on the method introduced by Brinker and co-workers (Lu et al., 1997). First, 60 ml tetraethoxyorthosilicate (TEOS, 98% Aldrich) and 63 ml ethanol (200 proof, Aldrich) were mixed well. 4.87 g of distilled water and 0.2 ml of 0.07M HCl solution were added under stirring. TEOS was hydrolyzed by refluxing for 1.5 h in silicone oil bath (60°C). Then, 4 g cetyltrimethylammonium bromide (CTAB, Aldrich) was transferred to 40 ml solution obtained in the first step. 7 ml of 0.07 M HCl was added to solution and the mixture was stirred continuously until surfactants were completely dissolved. Then the silica sol was aged by refluxing in silicone oil bath (50°C) around 2.5 days. The final molar composition was 1 SiO_2:8.1 EtOH: 4.9 H_2O:4.5×10^{-3} HCl. The silica sol was diluted 256:1 with anhydrous ethanol and was stored in a refrigerator for further use over several months.

2.2 Seed crystals

Three different types of zeolite seeds were hydrothermally synthesized. First, for *a*-oriented seed layer, two types of thin-along-a-axis MFI crystals are made using Bis-N,N-(tripropylammoniumhexamethylene)di-N,N-propylammonium (from now on, *trimer*-TPA) triiodide as structure directing agent (from now on, SDA). For one type, globular ~100 nm sized seeds were used (prepared as described below) while the other seeds were made in the absence of any seed. The synthesis solution was prepared by dissolving a specific amount of *trimer*-TPA in distilled water and KOH (1N solution, Aldrich) solution. The molar composition of solution was 40 SiO_2:5 *trimer*-$TPA^{3+}\cdot3I^-$:25 KOH:9500 H_2O. The mixture was stirred at room temperature overnight and then filtered (qualitative P8, Fisher Scientific) into 45-ml Teflon-lined stainless steel autoclaves (Parr Instrument Company) in laminar-flow hood. For seeded synthesis experiments, a certain amount of seed suspension of ~100 nm sized colloidal MFI crystals was

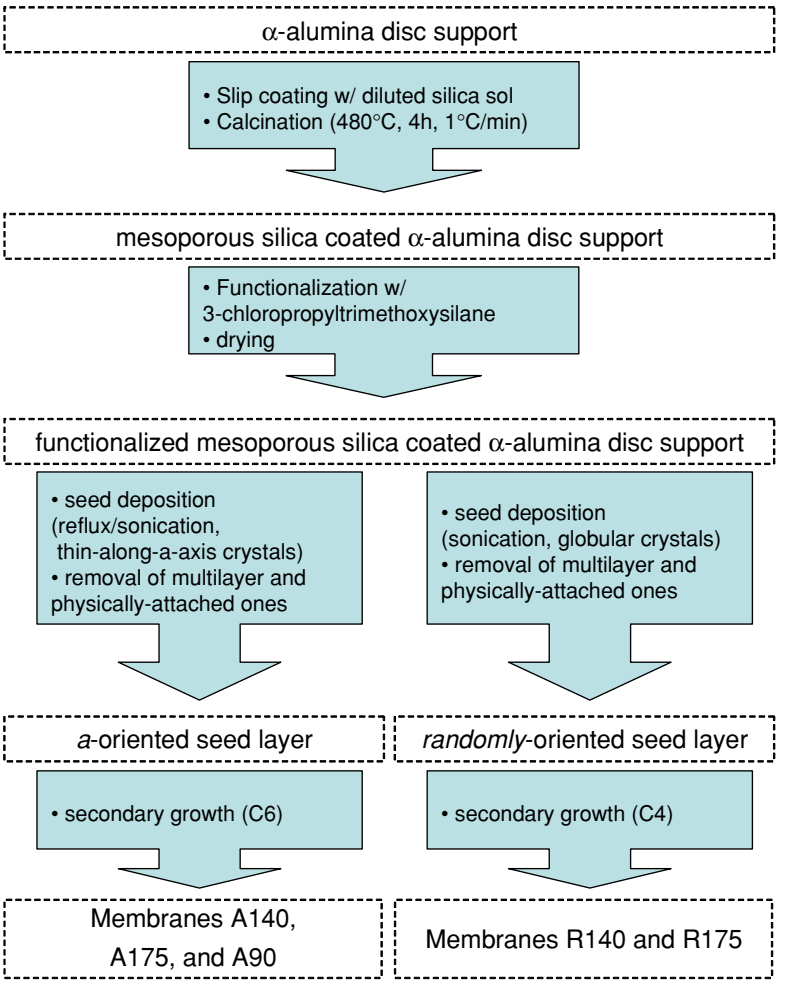

Seheme 1 Flowchart of process involved in making preferentially oriented MFI films from two different seed layers, i.e. *a*- and randomly oriented ones

added to the filtered mixture. The autoclaves were placed inside an oven preheated to 175°C equipped with a rotating rack. After 1 day, the reaction was quenched by tap water. The solid recovered by 5 times centrifugation was calcined at 525°C for 10 h with 1°C/min ramp rate under 150 ml/min air flow. When globular seeds were used the plate size was *ca.* 500–600 nm, while in the absence of the globular seed, $\sim$2 μm sized plates were obtained.

trimer-TPA triiodide was produced by exhaustive alkylation of bis(hexamethylene)trimamine with 1-iodopropane. X-ray diffraction, elemental and NMR analysis were described in detail elsewhere (Bonilla et al., 2004). Approximately 450 ml of the solvent 2-butanone (99.5%, Aldrich), an excess of 72.6 g of anhydrous potassium carbonate (99%, Fluka) (HI and water scavenger), and 27.87 g of the bis(hexamethylene)triamine (Aldrich) were added to a dry three-necked 1 L round flask. A dropping funnel and a reflux condenser were connected to the flask that contained a magnetic stirrer. The reaction flask was located in a silicone oil bath on a stirring hot plate, flushed with argon gas, and vented through a bubbler. While the solution was stirred, the whole system including the silicone bath, reaction flask, three necks, addition funnel was wrapped by aluminum foil to avoid iodide oxidation sensitive to light. 101 ml of 1-iodopropane (98%, Aldrich) was poured into the addition funnel quickly and added dropwise to the flask. During addition, the silicone oil bath was slowly heated to ca. 82°C. The reaction was started by refluxing under slow argon flow and was allowed to proceed for abut 15 h (overnight). The light yellow mixture was filtered to separate solids that precipitated in the bottom of funnel. The recovered solids contain the target product, *trimer*-$TPA^{3+}3I^{-}$ along with impurities, i.e., KI and

K_2CO_3. It was found that *trimer*-$TPA^{3+}3I^-$ is quite soluble in ethanol, whereas K_2CO_3 is insoluble and KI is slightly soluble in ethanol. The mixture was dissolved in 100 ml ethanol (200 proof, Fisher Scientific) for several hours followed by filtration to obtain filtrate. An off-white solid was obtained by removing ethanol by rotary evaporator. Then the solid was dissolved in 250 ml of 2-butanone and 250 ml of ethyl acetate was added slowly to precipitate out *trimer*-$TPA^{3+}3I^-$. After stirring for about 10 h the desirable product, *trimer*-$TPA^{3+}3I^-$, was recovered by vacuum filtration. For higher purity, the latter part (the cycle of ethanol extraction and recovery by butanone and ethyl acetate) was repeated.

100 nm sized globular seeds were synthesized based on a previous report (Lovallo and Tsapatsis, 1996). 0.85 g of NaOH (pellet, 99%, Aldrich) was mixed together with 60 ml 1 M TPAOH (1 M, Aldirch) in a plastic bottle. Then, 15 g of fumed silica (Cab-O-Sil) was added. The resulting slurry was heated around 80°C in a silicone oil bath until 10 g of water evaporated off. The final molar composition is 10 SiO_2:2.4 TPAOH:0.85 NaOH:86 H_2O. The mixture was transferred to Teflon-lined stainless steel autoclaves. The autoclaves were rotated in an oven preheated at 125°C. After 8 h, the autoclaves were cooled down by tap water. The solid product was obtained by 5 cycles of centrifugation and decantation and calcined as mentioned above. The seeds before seed deposition were stored in a drying oven set around 120°C.

2.3 Seed layer

Seed layer formation consists of two steps: (1) surface functionalization and (2) seed deposition (Ha et al., 2000). Thin-along-a-axis $\sim 2\,\mu$m MFI seeds were chemically attached onto the support in a reflux mode as described before (Choi et al., 2006). The surface of silica-coated α-alumina was functionalized with 3-chloropropyltrimethoxysilane (3CP-TMS 97%, Aldrich). 4 ml 3CP-TMS in argon-filled zip-lock bag was transferred by a syringe to anhydrous toluene (Aldrich) in specially designed glassware, where the α-alumina disc was placed vertically by use of Teflon holder (TH). Then, the glassware was heated by refluxing around 110°C under non-humid environment. After 3 h, the disc was taken out of the glassware and was placed in the drying oven ($\sim$120°C). 0.02 g of dried MFI crystals were placed in dry glassware and 40 ml anhydrous toluene were added under argon flow. Then, glassware was sealed with parafilm and sonicated for 10 min in ultrasonic bath (Branson 1210, 50/60 Hz) to disperse MFI seeds. After that, the α-alumina disc was placed horizontally on top of Teflon holder and it was heated to 110°C for 3 h. A brief sonication was used to eliminate multilayered and physically/weakly attached seeds. The disc was washed in toluene and stored in a drying oven ($\sim$120°C). Seeded substrates were heated up to 450°C with 1°C/min ramp rate and held for 4 h under 150 ml/min air flow.

For the formation of a monolayer of globular seeds or 500–600 nm sized thin-along-a-axis seeds, the sonication-assisted seed deposition method was used, adapted from a recent report (Lee et al., 2005). First, the surface of silica-coated α-alumina disc was functionalized with 3CP-TMS as described above. Then, 0.02 g of seeds were added to glassware and as for globular seeds, further dispersed in $\sim$50 ml anhydrous toluene by sonication for 1 h with glassware being sealed. The functionalized discs were stacked with cover glasses on both sides. The cover-glass sandwiched discs were placed vertically in a comb-shaped Teflon support. Then, while 10 min sonication was applied to the cover-glass sandwiched discs for thin-along-a-axis seeds, 2 min sonication was done for globular seeds (see Scheme 2 for arrangement). In addition, 2 min sonication was done to horizontally placed discs with silica-coated side facing upward (see Scheme 2 for arrangement). The discs were taken out of the glassware, washed in toluene, and dried in a drying oven ($\sim$120°C). Seeded substrates were calcined as described above.

2.4 Secondary growth

For secondary growth, a certain amount of TPAOH was well mixed with distilled water. TEOS was added as silica source. The mixture was fully hydrolyzed overnight. The molar composition was 40 or 60 SiO_2 :9 TPAOH:9500 H_2O (from now on, referred to C4 and C6, respectively) depending on seed layers. C4 composition was used for globular seeds following Gouzinis and Tsapatsis (1998) and C6 was utilized for thin-along-a-axis seeds in order to reduce nucleation rate as suggested by a recent study (Davis et al., 2006). The clear solution was filtered into Teflon-lined autoclaves where discs were already positioned tilted with seed layer side facing downward by use of Teflon holder.

Table 1 Summary of conditions used for MFI membranes reported here

	Seed deposition		Secondary growth			SEM	Out-of-plane
Sample No.	Method	Seeds	Composition	Temp. (°C)	Time (h)	Thickness (μm)	Orientation
A140-1	Reflux	Thin-along-a-axis, plate-like[a]	C6	140	11	~3	a
A140-2					18	~7	a
A140-3					24	~7.5	a
A140-4					48	~12	h0h/c/a
A175-1				175	4.5	~3	a
A175-2					6	~6	a
A175-3					24	~22	h0h/c/a
A90	Sonication	Thin-along-a-axis, plate-like[b]		90	93.5	N/A	a/h0h
R140		Globular	C4	140	24	~8	h0h/c
R175			C4	175	24	~15	c/h0h

[a]The size of seeds was ~2 μm along the *c*-axis.
[b]The size of seeds was ca. 500–600 nm along the *c*-axis.

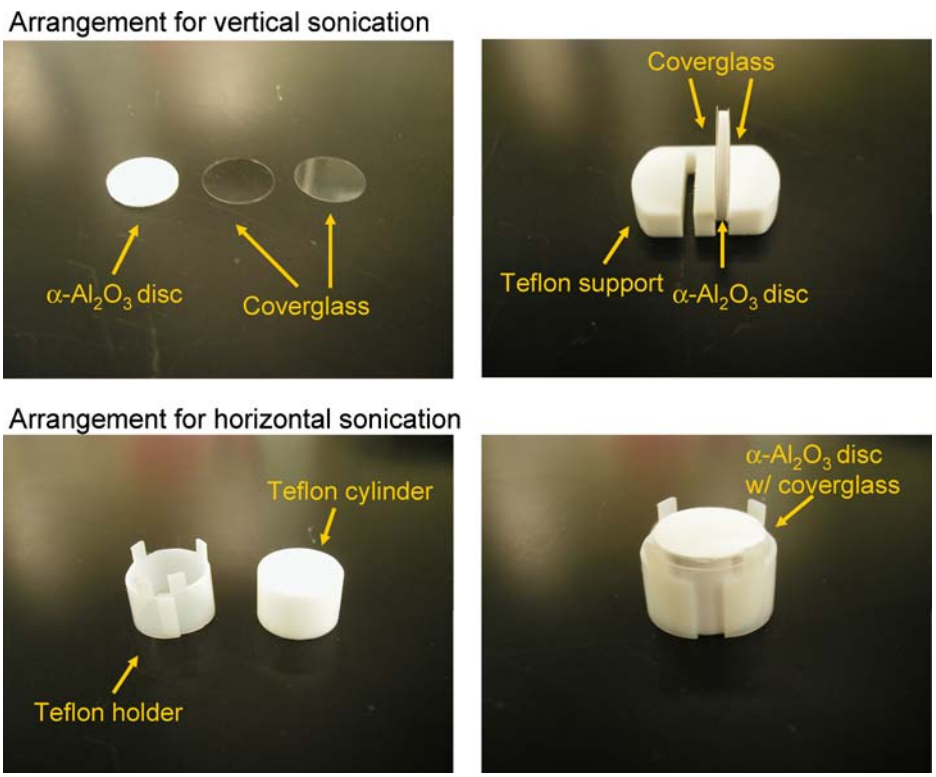

Seheme 2 Arrangements for vertical and horizontal sonication

The autoclaves were located in a preheated oven and reacted without agitation. Various times were used for secondary growth, mainly at three different temperatures (90°C, 140°C, and 175°C). After a certain time, the reaction was quenched by tap water. Discs taken out of autoclave were washed with tap water.

Different conditions involved in making samples are tabulated in Table 1.The MFI zeolite films were activated by burning off occluded TPA SDA through calcination. For calcination, membranes were heated up to 480°C with 0.5°C/min ramp rate and held for 4 h under 150 ml/min air flow.

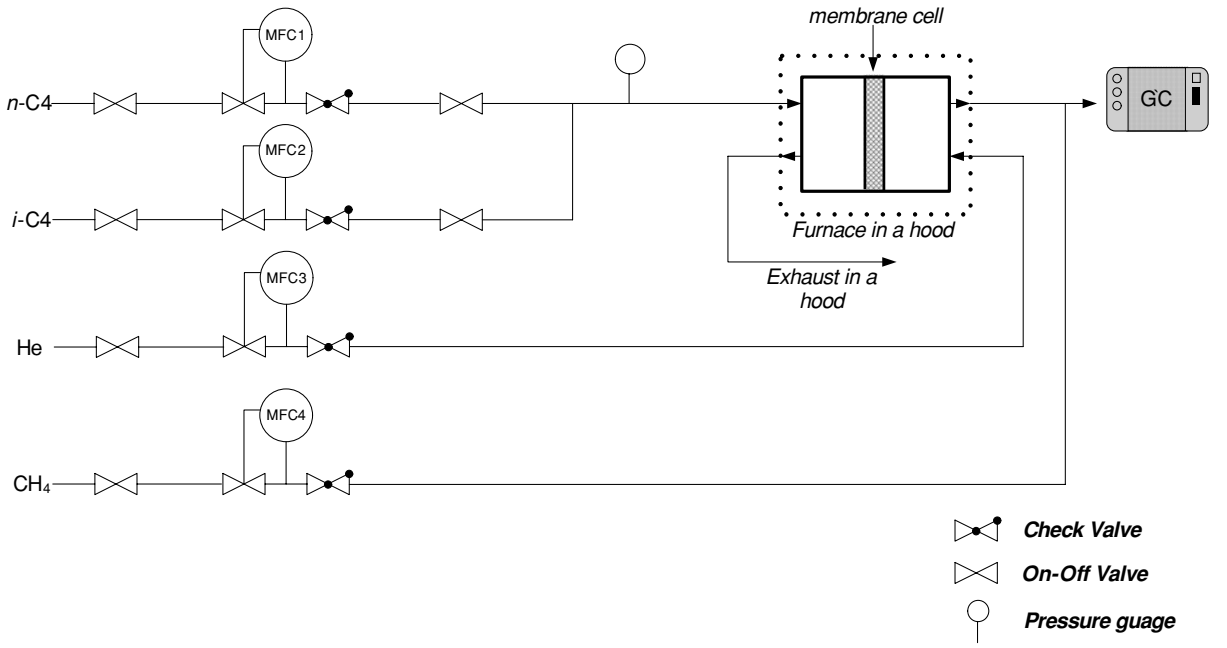

Seheme 3 Experimental setup for butane isomer gas (*n*-butane & *i*-butane) permeation measurements

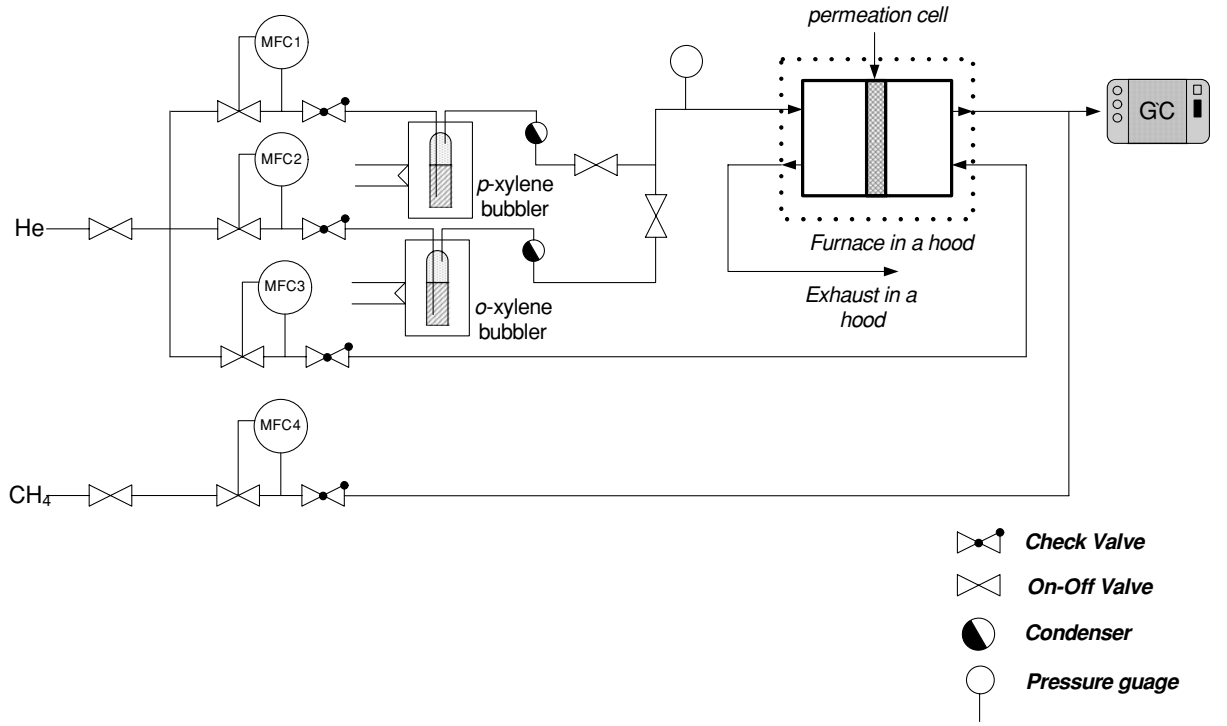

Seheme 4 Experimental setup for xylene isomer vapor (*p*-xylene & *o*-xylene) permeation measurements

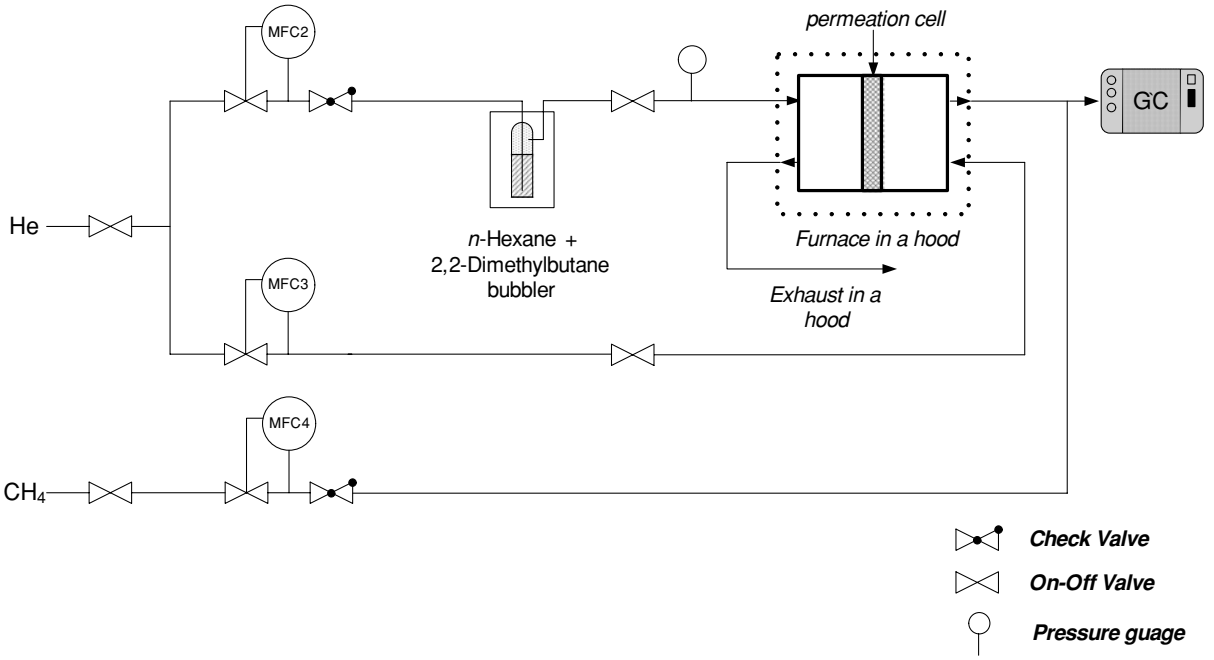

Seheme 5 Experimental setup for hexane isomer vapor (*n*-hexane & 2,2-dimethylbutane) permeation measurements

2.5 Microsturctural characterization

Scanning Electron Microscopy (SEM) was performed on JEOL 6500 microscope. Some of the samples were Pt-coated by sputtering before SEM imaging. Cross-section and top surface of samples were observed by SEM imaging. In addition, any preferred out-of-plane orientation was examined by X-ray Diffaction (XRD) on Bruker-AXS (Siemens) D5005 using 2.2 kW sealed Cu Source. The system was operated on a theta/2theta geometry.

2.6 Permeation measurements

Butane isomer gases (*n*- & *i*-butane), xylene isomer vapors (*p*- & *o*-xylene), and hexane isomer vapors (*n*-hexane & 2,2-dimethylbutane (referred to 2,2-DMB from now on) were used as binary mixture. The permeation systems for butane, xylene, and hexane isomers are illustrated in Scheme 3,Scheme 4, and Scheme 5,respectively. The permeation system was operated in Wicke-Kallenbach mode. That is, the total pressure in both feed and permeate sides was kept at 1 atm. A zeolite membrane on an α-alumina disc was mounted in a custom-made permeation cell with zeolite side facing the feed binary mixture. The permeation cell was sealed with Viton O-ring (McMaster). The entire permeation cell was inserted into a furnace (Thermolyne).

For butane permeation measurements, 50 kPa/50 kPa *n*- and *i*-butane isomers were fed through calibrated mass flow controller (MFC, MKS Instruments) continuously. The permeated butane gases were carried by He sweep gas. The permeate was sent to a gas chromatograph (GC, HP6890) equipped with a flame ionization detector (FID) for analysis. A 1/8″ SS packed column (0.19% picric acid on Graphpac, Alltech) was used and CH_4 reference gas was employed as internal standard.

For permeation measurements of xylene isomer vapors, two gas bubblers were used for each *p*- or *o*-xylene isomer. He carrier gas (∼20 ml/min) was independently fed through the each gas bubbler and oversaturated vapors were formed by circulating warm water (∼40°C) in the outside the bubblers. The oversaturated vapors were condensed in the condensers resulting in the equilibrated ca. 0.5 kPa *p*-xylene and

0.4 kPa *o*-xylene vapors. These vapors were mixed with He carrier gas and fed to the permeation cell. Susbsequently, the permeate was sent to GC (HP5890) equipped with FID detector using CH_4 gas as internal standard and a capillary column (EC-WAX, Alltech).

Finally, for permeation measurements of hexane isomers, liquid *n*-hexane and 2,2-DMB were

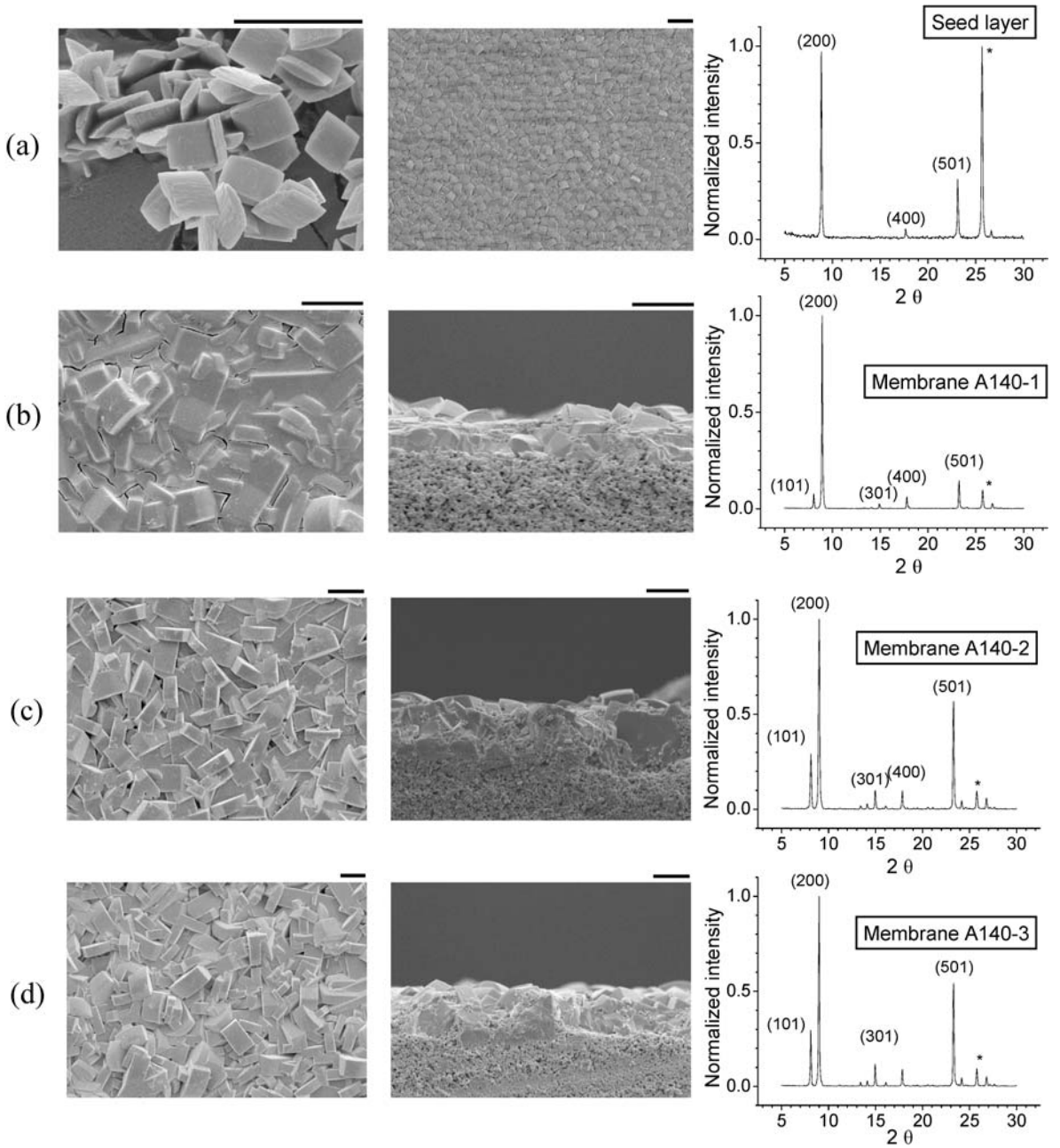

Fig. 1 (a) SEM of thin-along-a-axis, plate-like MFI seed crystals (shown on left) and SEM top view of covalently attached seed monolayer (*middle*) with corresponding XRD pattern (*shown on right*). (b–h) Top (*shown on left*) and cross section (*middle*) SEM images of membranes: (b) A140-1, (c) A140-2, (d) A140-3, (e) A140-4, (f) A175-1, (g) A175-2, and (h) A175-3 with corresponding XRD patterns (*right*). Scale bars correspond to 5 μm and the (*) in the XRD patterns marks α-Al_2O_3 peaks from the support. Synthesis conditions for membranes A140 and A175 are summarized in Table 1 *(Continued on next page.)*

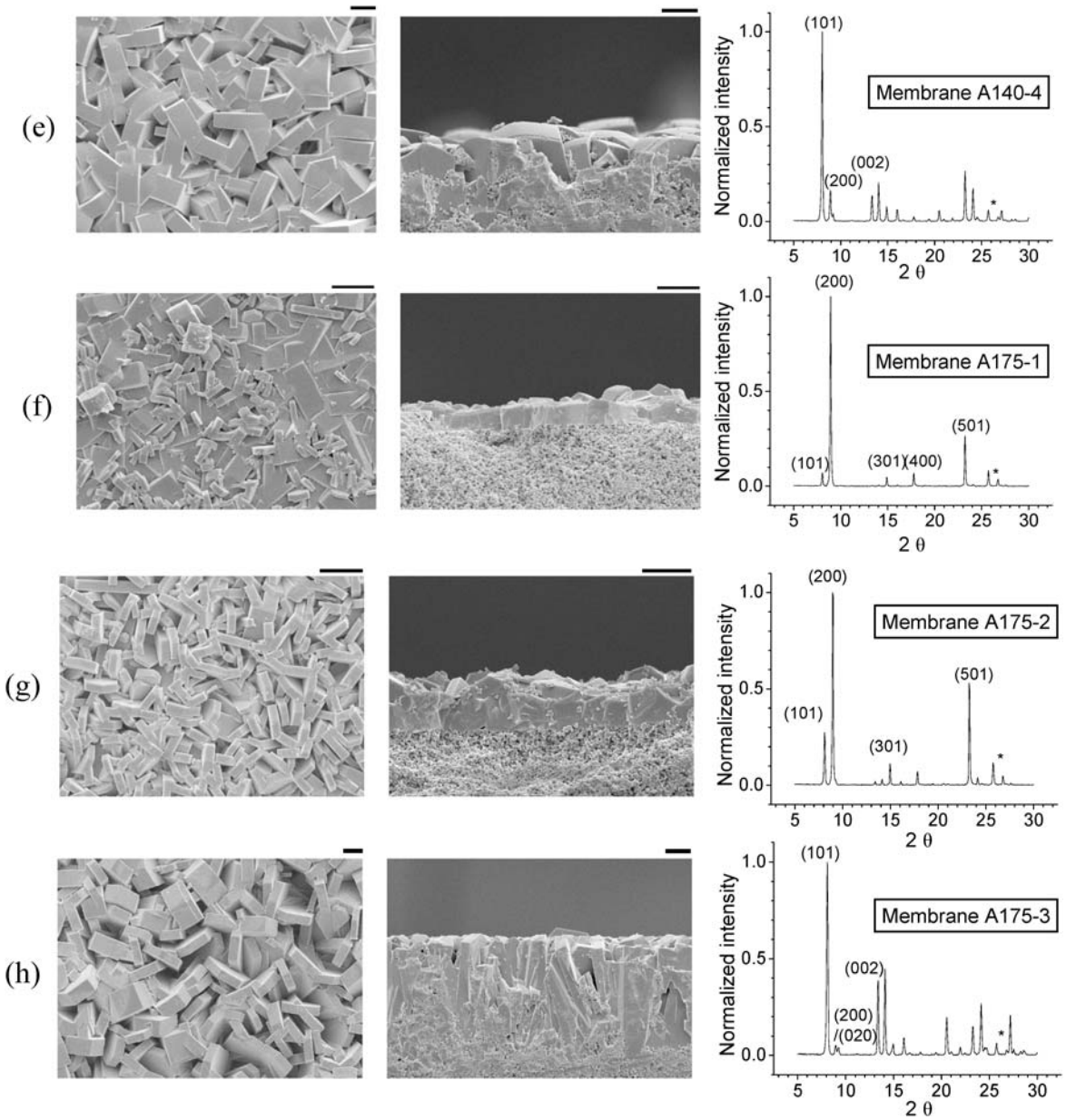

Fig. 1 *Continued.*

mixed in a gas bubbler. He carrier gas (∼30 ml/min) flowed through the gas bubbler resulting in ∼11 kPa *n*-hexane and ∼17 kPa 2,2-DMB and the mixture was fed to per meation cell. The permeated hexane isomers were detected using FID mode in GC in the same way as for butane isomers.

Permeance is defined as the value obtained dividing flux through membrane by pressure gradient. The units of permeance used here are mol/m^2·sec·Pa. The separation factor, SF, is expressed as,

$$\mathrm{SF} = \frac{y_{\mathrm{permeate}}/x_{\mathrm{permeate}}}{y_{\mathrm{feed}}/x_{\mathrm{feed}}}$$

where y_{feed} and x_{feed} are mole fractions of y and x in feed side, respectively, and y_{permeate} and x_{permeate} are mole fractions of y and x in permeate side, respectively with y being the faster permeating component (*n*-butane, *n*-hexane, or *p*-xylene).

3 Results and discussion

3.1 Membrane microstructure characterization

3.1.1 a-Oriented seed layers

Membranes A140, A175, and A90 were prepared starting from an *a*-oriented seed layer. Secondary growth was performed using composition C6 (60 SiO_2: 9 TPAOH:9500 H_2O) at 140, 175, and 90°C, respectively. For membranes A140 and A175, the seed layer was made from relatively large (∼2 μm in length) thin-along-a-axis MFI plates (Fig. 1(a))while for membrane A90, smaller (500–600 nm) thin-along-a-axis MFI plates made by seeded growth were used (not shown here). The small seed size leads to better substrate coverage and better intergrowth for small thickness, while it generates a larger number of grain boundaries. Membranes A140 and A175 were examined by SEM and XRD and the data are presented in Fig. 1. Membrane A140–1 is *a*-oriented and approximately 3 μm thick. However, it was not well intergrown with

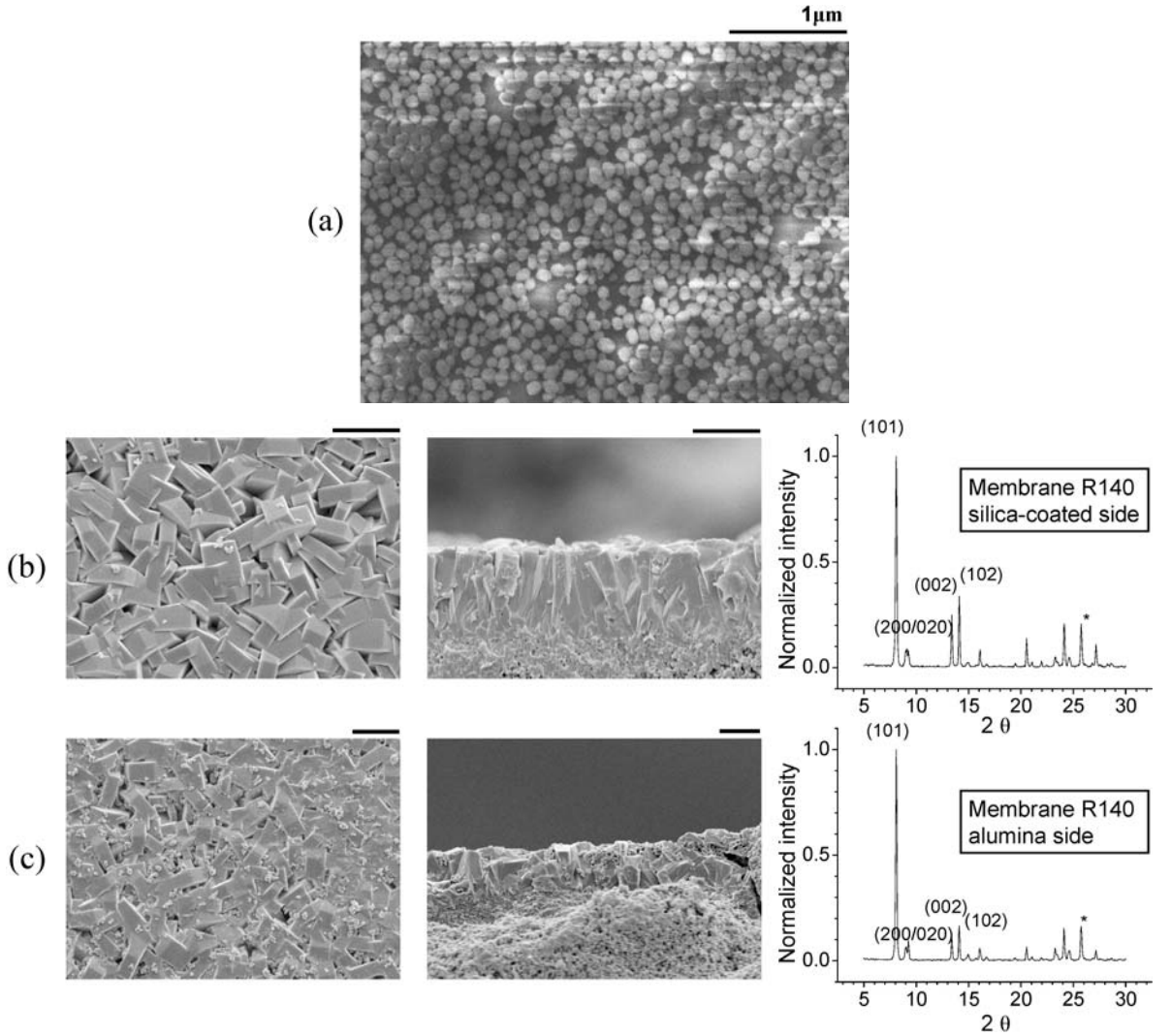

Fig. 2 (a) SEM image of globular nanocrystal seed monolayer formed by sonication-assisted covalent attachment. (b–e) Top (*left*) and cross section (*middle*) SEM images of (b) silica coated side of membrane R140, (c) alumina (*rough*) side of membrane R140, (d) silica coated side of membrane R175, and (e) alumina (*rough*) side of membrane R175. Scale bars correspond to 5 μm and the (*) in the XRD patterns marks α-Al_2O_3 peaks from the support. Synthesis conditions for membranes R140 and R175 are summarized in Table 1 (*Continued on next page.*)

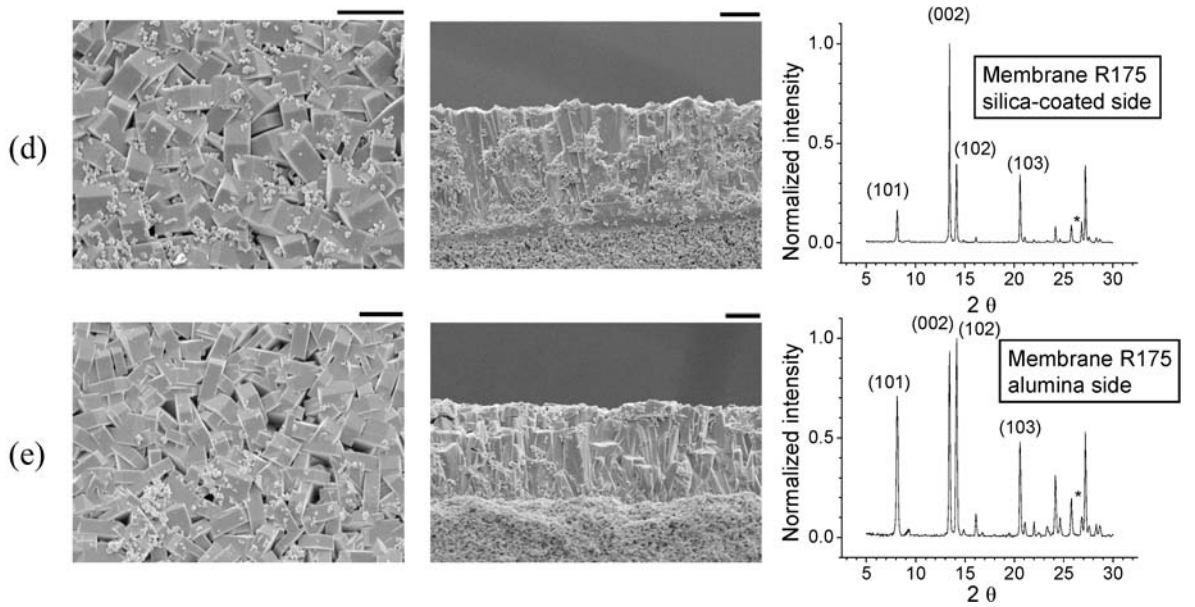

Fig. 2 *Continued.*

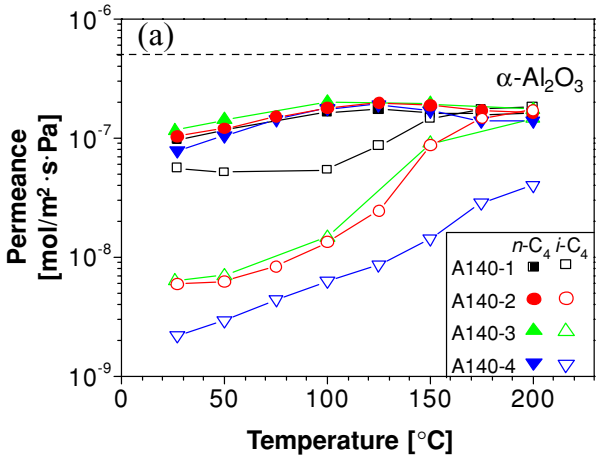

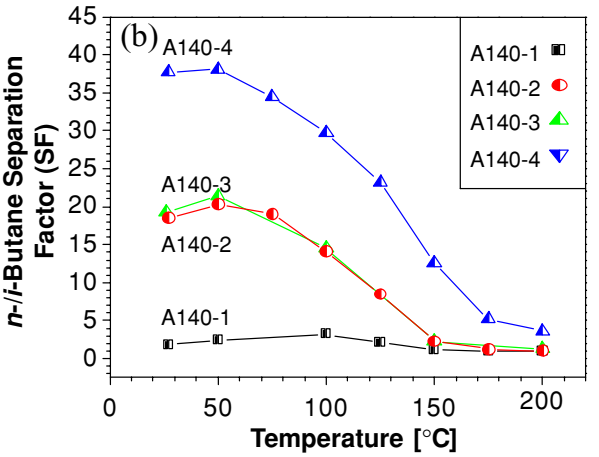

Fig. 3 (a) *n*-Butane (*filled symbols*) and *i*-butane (*open symbols*) permeance and (b) *n*-butane/*i*-butane separation factor (*semi-filled symbols*) vs. temperature for 50%/50% butane isomer feed through membranes A140–1, A140-2, A140-3, and A140-4. Dashed line represents the permeance of *n*-butane through an α-Al_2O_3 disc

cracks visible in top view SEM (Fig. 1(b)). Membranes A140-2 and A140-3 prepared by secondary growth at 140°C for 18 and 24 h have very similar microstructure. They are both ~7 μm thick and predominantly *a*-oriented with some *h0h*-out-of-plane component due to nucleated crystals. The larger *a*-out-of-plane oriented grains along with the smaller *h0h*-oriented grains can be easily distinguished in the top view SEM images (Fig. 1(c) and (d)). After prolonged secondary growth (48 h) at 140°C, membrane A140-4 has a total thickness of 12 μm including a columnar *h0h*-oriented overlayer (Fig. 1(e)). From these data, it is evident that during secondary growth of *a*-oriented seed layers at 140°C, growth of existing seeds competes with nucleation and growth of new initially randomly oriented crystals. These new crystals eventually develop a columnar *h0h*-oriented film following the van der Drifts growth mechanism (Gouzinis and Tsapatsis, 1998). Such

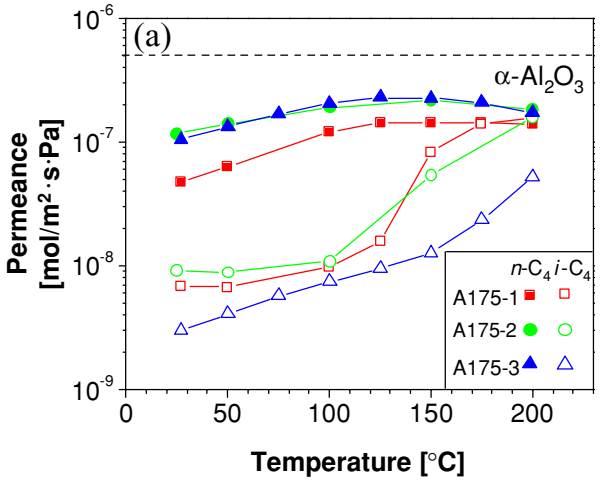

Fig. 4 (a) *n*-Butane (*filled symbols*), *i*-butane (*open symbols*) permeance and (b) *n*-butane/*i*-butane separation factor (*semi-filled symbols*) vs. temperature for 50%/50% butane isomer feed through membranes A175-1, A175-2, and A175-3. Dashed line represents the permeance of *n*-butane through an α-Al_2O_3 disc

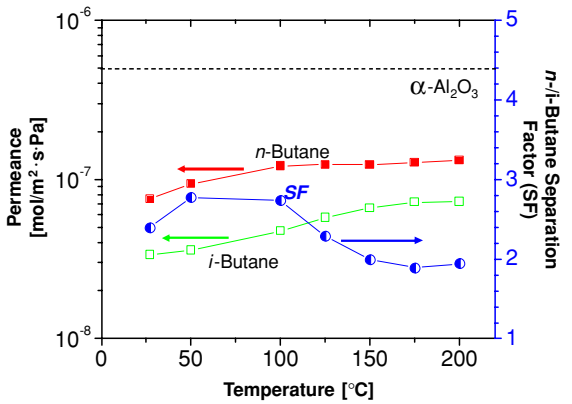

Fig. 5 *n*-Butane (*filled symbols*), *i*-butane (*open symbols*) permeance and *n*-butane/*i*-butane separation factor (*semi-filled symbols*) vs. temperature for 50%/50% butane isomer feed through membrane A90. Dashed line represents the permeance of *n*-butane through an α-Al_2O_3 disc

competition was also observed for the case of *b*-oriented MFI films (Lai et al., 2003; Lai and Tsapatsis, 2004; Lai et al., 2004).

Secondary growth at 175°C follows a similar trend in resulting microstructures with one difference being the required growth time. Membrane A175-1, grown for 4.5 h, is well intergrown and highly *a*-oriented (Fig. 1f). After 6 h of growth (A175-2), an *h0h*-orineted layer starts to emerge and evolves into a well intergrown thick columnar *h0h*-oriented film after 24 h (A175-3) as evident in Fig. 1(g) and (h).

An *a/h0h*-oriented membrane can also be prepared using smaller seeds and secondary growth at 90°C for 93.5 h (not shown here).

3.1.2 Randomly oriented seed layers

It is well established that *c*- and *h0h*-oriented layers can be prepared starting from randomly oriented seeds and growing under conditions that favor fast growth along the *c*-axis (Deckman et al., 1996; Lovallo and Tsapatsis, 1996; Verduijn et al., 1996; Gouzinis and Tsapatsis, 1998; Lovallo et al., 1998; Xomeritakis et al., 1999; Xomeritakis et al., 2000; Bonilla et al., 2001; Bons and Bons, 2003). Since *c*-axis is the favored crystallographic growth direction for TPA-MFI (de Vos Burchart et al., 1993; Bonilla et al., 2004), this preferred orientation can be readily obtained for thick MFI films. Membranes R140 and R175, made from mono-layered randomly oriented seeds (Fig. 2(a))have well intergrown similarly oriented films on both sides (Fig. 2(b)–(e)). This can be attributed to the seeding by sonciation-assisted method that, unlike casting or seeding by reflux, does not limit the seed layer formation to only one side of the support. Membrane R140 is *h0h*-/*c*-oriented 8 μm thick while membrane R175 is *c*-/*h0h*-oriented and 15 μm thick. These microstructures are very similar to previously obtained columnar films (Xomeritakis et al., 1999; Xomeritakis et al., 2000). One minor difference is the more pronounced *h0h*-component which

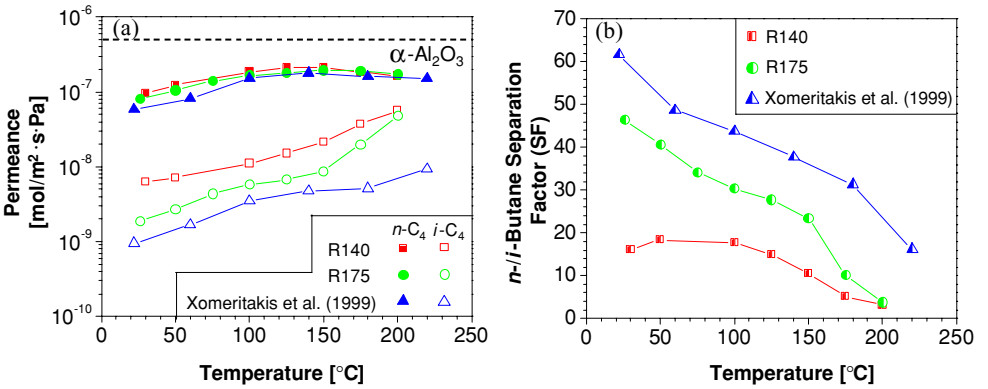

Fig. 6 (a) *n*-Butane (*filled symbols*), *i*-butane (*open symbols*) permeance and (b) *n*-butane/*i*-butane separation factor vs. temperature for 50%/50% butane isomer feed in membranes R140, R175 and one *c*-oriented MFI membrane from previous report: (Xomeritakis et al., 1999). Dashed line represents the permeance of *n*-butane through an α-Al_2O_3 disc

may be attributed to the less packed monolayer obtained in the present study as opposed to the closed packed multi-layers obtained by slip casting in our previous work (Xomeritakis et al., 1999; Xomeritakis et al., 2000).

3.2 Permeation measurements

3.2.1 n-/i-butane

Figure 3 shows the *n*- and *i*-butane permeances through membranes A140. As expected from the high density of cracks evident by SEM (Fig. 1(b)), A140-1 shows hardly any *n*-/i-butane selectivity. The *a*-oriented membranes A140-2 and A140-3 essentially show identical behavior as expected from their similar microstructures as revealed by SEM and XRD (Fig. 1(c) and (d)). The separation factor increases further when the membrane becomes thicker (A140-4) with the growth of the *h0h*-oriented overlayer as shown in Fig. 1(e). For this membrane, a separation factor as high as 4 is observed at high temperature of up to 200°C.

Figure 4 shows *n*- and *i*-butane permeances through membranes A175. A similar trend is observed, i.e., separation factor increased with film thickness and growth of the *h0h*-oriented overlayer. The separation factor for membrane A90 is around 3 at low temperature but it is preserved at a value of about 2 at temperature as high as 200°C as shown in Fig. 5.

It is worth pointing out that *n*-butane permeance is essentially identical for all of the above membranes (with the exception of A175-1) and any increase of separation factor is due to the decrease in *i*-butane permeance. There are several factors that may contribute to this behavior. First, we point out that the *n*-butane permeance through the α-Al_2O_3 support is only higher by a factor of 2 than the measured membrane permeances. It is therefore possible that for some of the thinner *a*-oriented membranes, higher *n*-butane flux and correspondingly high separation factors could be obtained had we used a higher flux support. Second, it is evident by SEM that micrometer scale gaps exist between the grains in the membranes especially in the *h0h*-oriented overlayer. These gaps are formed due to the fast out-of-plane growth in comparison to in-plane growth rate. Therefore the SEM thickness is probably not indicative of actual diffusion lengths through the membrane. These results show that *a*-oriented MFI films can be *n*-/*i*-butane selective and performance improvements may be possible by growing thinner films in high flux supports.

Figure 6 shows the *n*-/*i*-butane performance for membranes made from randomly oriented seed layers. The behavior is very similar to that of *c*-oriented membranes reported by Xomeritakis et al. (1999). Despite the presence of deposit on both sides of the α-Al_2O_3 support, the *n*-butane permeance is at the same level with that reported previously from membranes grown only on the polished and silica coated side of the α-Al_2O_3 disc.

Figure 7 shows collective results regarding MFI membrane performance including the *a*-oriented membranes of this study along with *b*- and *c*-oriented films. Table 2 lists additional information regarding the membranes used in Fig. 7. With the exception of the thin membranes on high flux supports prepared by

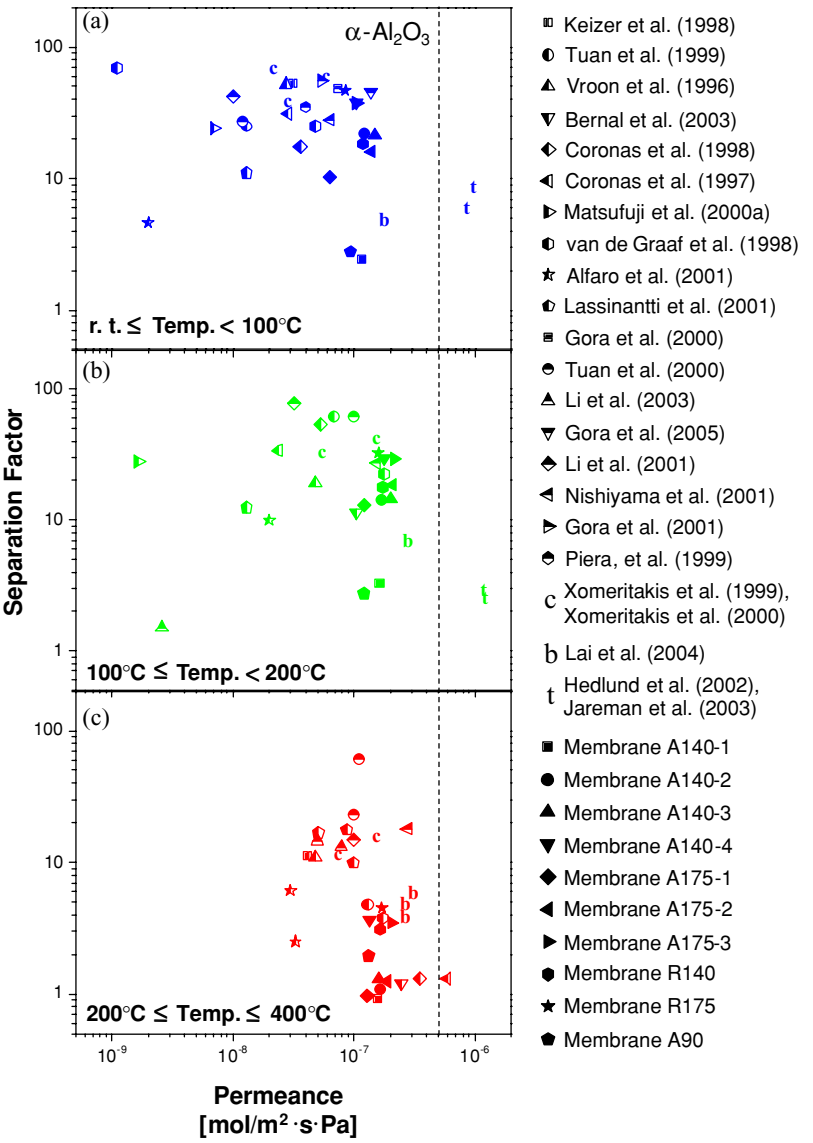

Fig. 7 *n*-Butane/*i*-butane separation factor vs. *n*-butane permeance for MFI membranes at various temperature ranges: (a) from room temperature to 100°C, (b) between 100°C and 200°C, and (c) from 200°C to 400°C. Filled symbols are from membranes prepared in this study, semi-filled symbols correspond to literature reference, and the letters (a, b, and c) indicate the corresponding out-of-plane preferred orientation. The symbol t indicates the performance of 0.5 μm thick MFI films grown on high flux supports. Dashed line represents the permeance of *n*-butane through an α-Al_2O_3 disc. See Table 2 for details on the data used

Hedlund and coworkers (Hedlund et al., 2002; Jareman et al., 2003), permeances appear to be clustered around 10^{-7} mo/m$^2 \cdot$ s $\cdot$ Pa, while separation factors vary considerably. Micron thick *b*-oriented films exhibit higher permeances but lower separation factors (below 10) compared to thick *c*-oriented columnar membranes that have separation factors larger than 10 and approaching to $\sim$100 at room temperature. The MFI films, made from *a*-oriented seed layers from the current study, indicate an intermediate behavior between that of *c*- and *b*-oriented films. More specifically, their separation factors are higher than those of the thin *b*-oriented membranes and lower than those of the several micron thick columnar *c*- or *h0h*-oriented films.

Neglecting the differences in preferred orientation, one may correlate the *n*-/*i*-butane separation factor with membrane thickness. More specifically, it appears that thicker membranes with columnar grains are more *n*-butane selective compared to the thinner films consisting of rather isometric grains. The differences become more pronounced at lower temperatures indicating that adsorptive behavior is a strong contribution factor.

It is obvious that *c*- or *h0h*-preferetially oriented thick columnar films, made from randomly oriented

Table 2 Additional information for the MFI membranes used in Fig. 7

Membrane (Si/Al)/support with pore size	T (K)	P[a]	SF[b]	Mode[c]	Orientation[d]	t[e]	Ref.
Silicalite-1 (∞)/α-Al_2O_3 disc	298	0.3	52[f]	WK	r	$\sim$7[g]	(Keizer et al., 1998)
(home-made) 135–165 nm	473	0.4	11[f]				
Silicalite-1 (∞)/α-Al_2O_3 disc	323	1.8	5	WK	b	1	(Lai and Tsapatsis, 2004)
(home-made) 150–200 nm	373	2.8	7				
	493	2.7	5				
	493	2.7	4				
	493	3.1	6				
Silicalite-1 (∞)/α-Al_2O_3 disc	295	0.6	61.8	WK	c	30	(Xomeritakis et al., 1999)
(home-made) 150 nm	373	1.5	43.7				
	493	1.5	16.2				
	295	0.2	71			15	(Xomeritakis et al., 2000)
	295	0.3	40.3			30	
	373	0.6	34.1				
	493	0.8	12				
Silicalite-1 (∞)/α-Al_2O_3 disc	298	9.8	9	WK	r	0.5	(Hedlund et al., 2002)
(Inocermic GmbH) 100 nm top layer	433	12	3[f]				
ZSM-5 (600)/α-Al_2O_3 tube	301	0.1	25[f]	PG	r	40	(Tuan et al., 1999)
(US Filter) 200 nm	373	0.7	62[f]				
	473	1.3	4.8[f]				
Silicalite-1 (∞)/α-Al_2O_3 disc	298	0.3	52	WK	r	5	(Vroon et al., 1996)
(home-made) 135–165 nm	373	0.5	19				
	473	0.5	11				
ZSM-5 (600)/γ-Al_2O_3 tube	298	0.4	17.5	WK	r	$\sim$20[h]	(Bernal et al., 2003)
(SCT^{TM}) 5 nm	393	1.1	11.4				
	493	2.5	1.2				
ZSM-5 (100)/γ-Al_2O_3 tube	335	0.3	31	PG	N/A	20$\sim$25[i]	(Coronas et al., 1998)
(US Filter) 5 nm	394	0.5	54[f]				
	487	3.5	1.3[f]				
ZSM-5 (100)/γ-Al_2O_3 tube	343	0.1	24	PG	N/A	20$\sim$25	(Coronas et al., 1997)
(US Filter) 5 nm	370[j]	0.2	34				
	510	5.9	1.3				
ZSM-5 (500)/α-Al_2O_3 disc	300	0.01	69	N/A	b	40[k]	(Matsufuji et al., 2000a)
(NGK Insulators Ltd.) 100 nm	375	0.02	28				
ZSM-5 (100)/α-Al_2O_3 disc	298	8.7	6.2	WK	r	0.5	(Jareman et al., 2003)
(Inocermic GmbH) 100 nm top layer	413	12.4	2.6[f]				
Silicalite-1 (∞)/SS disc	303	0.5	24.9[l]	WK	N/A	30$\sim$50	(van de Graaf et al., 1998)
(Krebsöge Sika-RF) 7–8 μm	406	1.8	22.5				
	494	1.7	3.78				
Silicalite-1 (∞)/SS tube	298	0.02	4.6	WK	r	$>$100	(Alfaro et al., 2001)
(Mott) 500 nm	373	0.2	10				
	503	0.3	6.1				
	603	0.3	2.5				
ZSM-5 (50)/α-Al_2O_3 disc	348	0.1	11	WK	(051) (133)	$\sim$2	(Lassinantti et al., 2001)
(Inocermic GmbH) 100 nm top layer	433	0.1	12.4				
	493	0.5	16.7				
	593	1.0	10				
	500	0.9	17.8				

(*Continue on next page.*)

Table 2 Continue

Membrane (Si/Al)/support with pore size	T (K)	P[a]	SF[b]	Mode[c]	Orientation[d]	t[e]	Ref.
Unsupported silicalite-1 (∞)	298	0.8	48	WK	N/A	50	(Gora et al., 2000)
ZSM-5 (100)/γ-Al_2O_3 tube (SCT) ~5 nm	298	0.4	35	N/A	N/A	20~25[i]	(Piera et al., 1999)
B-ZSM-5 (Si/B = 12.5)/α-Al_2O_3 tube (U.S. Filter) 200 nm inner layer	300	0.1	27	WK	r	85~100[m]	(Tuan et al., 2000)
	433	1.0	62[f]				
	473	1.1	61				
	527	1.0	23[f]				
ZSM-5 (120)/α-Al_2O_3 disc (NGK Insulators Ltd) 100 nm top layer	443	0.03	2	WK	r	<2	(Li et al., 2003)
	613	0.5	15				
	673	0.8	13				
Silicalite-1 (∞)/TiO_2/SS tube (Trumen^{TM}) 100 nm top layer	303	1.4	45	WK	N/A	15	(Gora and Jansen, 2005)
ZSM-5[n](50)/α-Al_2O_3 tube ~2 μm	303	0.1	42	WK	r	7	(Li et al., 2001)
	373	0.3	78				
	473	1.0	15				
Silicalite-1 (∞)/TiO_2/SS disc (Trumen^{TM}) 100 nm top layer	303	0.7	28	WK	N/A	30[o]	(Nishiyama et al., 2001)
	373	1.6	27				
	478	2.8	18				
Silicalite-1 (∞)/TiO_2/SS disc (Trumen^{TM}) 100nm top layer	303	0.5	55	WK	N/A	35[o]	(Gora et al., 2001)
Silicalite-1 (∞)/α-Al_2O_3 disc (home-made) 150~200 nm	323	1.17	2.4	WK	a	~3	A140-1
	373	1.65	3.2				
	473	1.60	0.93				
	323	1.21	20.3	WK	a	~7	A140-2
	373	1.79	14.1				
	473	1.65	1.0				
	323	1.42	21.4	WK	a	~7.5	A140-3
	373	2.03	14.5				
	473	1.74	1.3				
	323	1.06	38.1	WK	h0h/c/a	~12	A140-4
	373	1.78	29.8				
	473	1.39	3.65				
	323	0.64	10.1	WK	a	~3	A175-1
	373	1.21	13.0				
	473	1.41	0.96				
	323	1.41	16.8	WK	a	~6	A175-2
	373	1.91	18.4				
	473	1.85	1.25				
	300	1.05	37.2	WK	h0h/c/a	~22	A175-3
	373	2.06	29.2				
	473	1.74	3.5				
	323	0.9	2.78[f]	WK	a/h0h	N/A	A90
	373	1.2	2.73[f]				
	473	1.32	1.94[f]				
	323	1.24	18.4[f]	WK	h0h/c	~8	R140
	373	1.86	17.7[f]				
	473	1.64	3.1				

(*Continue on next page.*)

Table 2 Continue

Membrane (Si/Al)/support with pore size	T (K)	P^a	SF[b]	Mode[c]	Orientation[d]	t^e	Ref.
	299	0.81	46.5[f]	WK	c/hoh	∼15	R175
	373	1.67	30.4[f]				
	473	1.71	3.8[f]				

[a]*n*-Butane permeance in 10^{-7} mol/m^2 sec Pa.
[b]*n*-Butane/*i*-butane separation factor
[c]Mode: permeation mode (Wicke-Kallenbach mode (WK) or pressure gradient mode (PG)).
[d]Orientation represents an out-of-plane orientation of membranes with r (randomly oriented), b (*b*-oriented), a (*a*-oriented), c (*c*-oriented), h0h (*h0h*-oriented) and so on.
[e]Thickness in μm.
[f]*n*-/*i*-Butane separation factors are displayed in the inset of Fig. 9 along with corresponding *n*-hexane/2,2-DMB separation factors (from Table 3) in the same temperature range.
[g]The thickness is obtained from Vroon et al., 1998.
[h]The thickness of H-ZSM5 membrane is estimated from growth rate of Na-ZSM5 membrane reported by Tuan et al., 1999.
[i]The thickness is obtained from Coronas et al., 1997.
[j]Data at 370 K are displayed in the temperature range of 100°C ≤ Temp. < 200°C (Green color) in Fig. 6(b).
[k]The thickness is obtained from Matsufuji et al., 2000b.
[l]Separation factor at 303 K is an average of three different values.
[m]The thickness is obtained from Gade et al., 2001.
[n]*n*-Butylamine is used as SDA instead of tetrapropylammnonium cation (TPA).
[o]The thickness of membranes is from in Table 2 of Gora and Jansen, 2005.

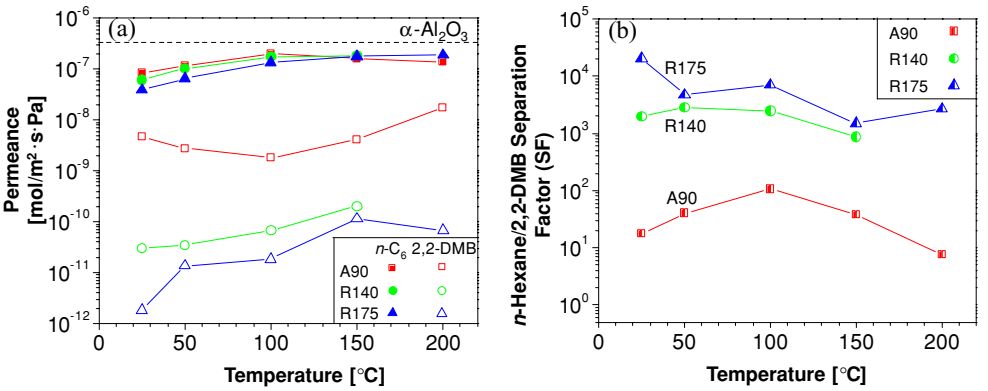

Fig. 8 (a) *n*-Hexane (*filled symbols*), 2,2-DMB (*open symbols*) permeance and (b) *n*-hexane/2,2-DMB separation factor (*semi-filled symbols*) vs. temperature for membranes R140, R175 and A90. Dashed line represents the permeance of *n*-hexane through an α-Al_2O_3 disc

seed layers, show the highest separation factor for *n*-/*i*-butane. However, until *a*-, *b*-, and *c*-oriented films with similar thickness and grain structure can be made and compared, one cannot conclude regarding the contribution of preferred orientation vs. other factors like membrane thickness and grain boundary structure to the above differences.

3.2.2 n-hexane/2,2-DMB

Given the performance for *n*-/*i*-butane separation, we can expect that thick columnar *c*-oriented films will perform better than thinner *a*/*h0h*-oriented films for *n*-hexane/2,2-DMB. This expectation is confirmed by the experimental results of Fig. 8.Membranes R175 and R140 show higher separation factors and comparable *n*-hexane flux compared to membrane A90. The collective results of Fig. 9 show that membranes R175 and R140 have the highest reported separation factor for *n*-hexane/2,2-DMB. Also, the inset of Fig. 9 confirms that for most MFI membranes, there is a correlation between *n*-/*i*-butane and n-hexane/2,2-DMB separation factors. Detailed information of the membranes used in Fig. 9 is summarized in Table 3.

Table 3 Additional information for the MFI membranes used in Fig. 9

Membrane (Si/Al)/support with pore size	T (K)	P[a]	SF[b]	Mode[c]	Orientation[d]	t[e]	Ref.
Silicalite-1(∞)/α-Al_2O_3 disc	298	0.1	600[f]	WK	r	7[g]	(Keizer et al., 1998)
(home-made) 135∼165 nm	473	0.3	2000[f]				
Silicalite-1 (∞)/α-Al_2O_3 disc	373	5.4	76[f]	WK	r	0.5	(Hedlund et al., 2002)
(Inocermic GmbH) 100 nm top layer	663	5.6	227				
B-ZSM-5 (Si/B = 12.5)/α-Al_2O_3 tube	373	1.5	2280[f]	WK	r	85∼100	(Gade et al., 2001)
(U.S. Filter) 200 nm	523	1.0	5[f]				
B-ZSM-5 (Si/B = 12.5)/SS tube	373	1.5	1950				
(Mott Metallurgical) 500 nm	523	1.5	72				
B-ZSM-5 (Si/B = 100)/SS tube	373	1.3	921	PG	r	85∼100[h]	(Arruebo et al., 2006)
(Pall Corp.) 800 nm							
Silicalite-1 (∞)/SS tube (Pall Corp.) 800 nm	373	2.5	563				
ZSM-5 (100)/γ-Al_2O_3 tube (US Filter) ∼5 nm	374	0.2	500[f]	WK	N/A	20∼25[j]	(Coronas et al., 1998)
	463[i]	0.8	0.9[f]				
Silicalite-1 (∞)/α-Al_2O_3 disc	373	6.3	47[f]	WK	r	0.5	(Jareman et al., 2003)
(Inocermic GmbH) 100 nm top layer	648	5.2	88				
ZSM-5 (600)/α-Al_2O_3 tube 200 nm	300	0.2	100[f]	WK	r	N/A	(Flanders et al., 2000)
	375	2.0	1260[f]				
	520	1.6	8[f]				
ZSM-5[k] (500)/α-Al_2O_3 disc	303	0.02	120	PV	b	40	(Matsufuji et al., 2000c)
(NGK Insulators, Ltd.) 100 nm							
ZSM-5 (100)/α-Al_2O_3/γ-Al_2O_3 tube	358	1.0	680	WK	r	25∼30	(Gump et al., 1999)
(US Filter) 5 nm inside layer	373	1.3	750				
B-ZSM-5 (Si/B = 100)/SiC/γ-Al_2O_3	436	0.34	247	WK[l]	N/A	35∼150	(Kalipcilar et al., 2002)
monolith 5 nm on γ-Al_2O_3	497	0.28	171				
Silicalite-1 (∞)/γ-Al_2O_3 tube	363	1.8	22.5	WK	r	2∼10	(Funke et al., 1997)
(US Filter) ∼5 nm	370	1.9	21.1				
	407	2.1	2.1				
Silicalite-1 (∞)/α-Al_2O_3 disc	323	1.15	40[f]	WK	a/h0h	N/A	A90
(home-made) 150∼200 nm	373	2.00	105.8[f]				
	473	1.38	7.54[f]				
	323	1.03	2830[f]	WK	h0h/c	∼8	R140
	373	1.77	2490[f]				
	298	0.39	203300[m,f]	WK	c/h0h	∼15	R175
	323	0.66	4700[f]				
	373	1.35	6990[f]				
	473	1.89	2660[f]				

[a] n-hexane permeance in 10^{-7} mol/m^2 sec Pa.
[b] n-Hexane/2,2-DMB separation factor.
[c] Mode: permeation mode (Wicke-Kallenbach mode (WK), pressure gradient mode (PG), and pervaporation (PV)).
[d] Orientation represents an out-of-plane orientation of membranes with r (randomly oriented), a (*a*-oriented), c (*c*-oriented), and h0h (*h0h*-oriented).
[e] Thickness in μm.
[f] n-Hexane/2,2-DMB separation factors are displayed in the inset of Fig. 9 along with corresponding n-/i-butane separation factors (from Table 2) in the same temperature range.
[g] The thickness is obtained from Vroon et al., 1998.
[h] The thickness is obtained from Gade et al., 2001.
[i] Data at 463 K are displayed in the temperature range of 200°C ≤ Temp. ≤ 390°C (Red color) in Fig. 8.
[j] The thickness is obtained from Coronas et al., 1997.
[k] The membrane is tested for mixture of n-hexane and 2,3-(not 2,2) dimethylbutane and the permeance of n-hexane was obtained by dividing the pervaporation flux by the vapor pressure at room temperature.
[k] The pressure in both sides of permeation system was maintained at 83 kPa.
[m] 2,2-DMB in the permeate side was not detected by GC. But separation factor was obtained considering the permeance of 2,2-DMB equal to that from the lowest detection limit of GC.

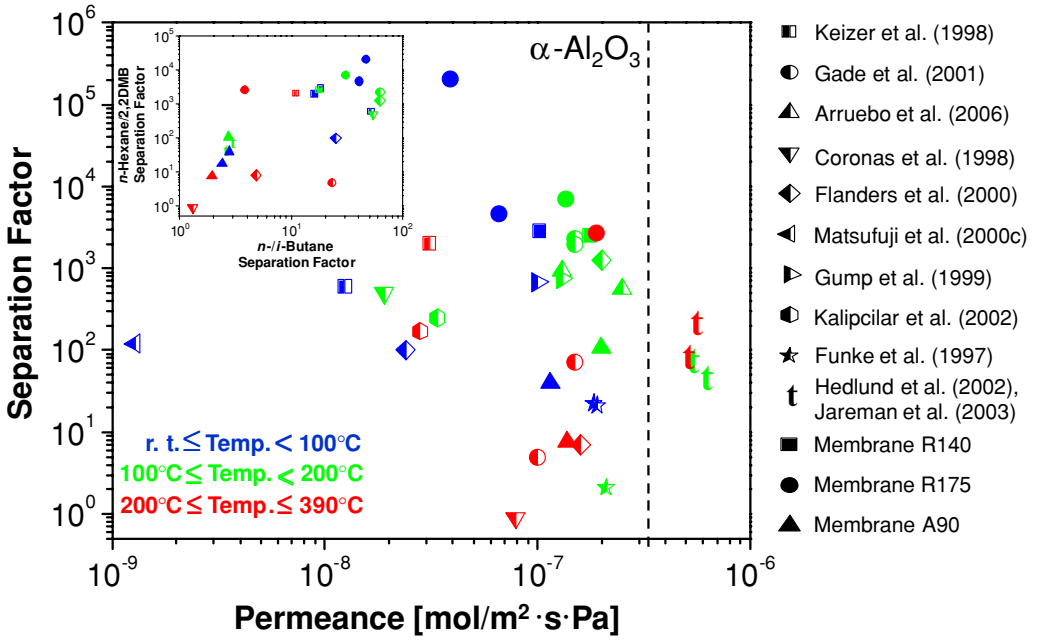

Fig. 9 *n*-Hexane/2,2-DMB separation factor vs. *n*-hexane permeance for MFI membranes at various temperature ranges : blue symbols correspond to measurements from room temperature to 100°C, green from 100°C to 200°C, and red from 200°C to 390°C. *n*-Hexane/2,2-DMB vs *n*-/*i*-butane separation factor is given in the inset. Filled symbols are from membranes prepared in this study, semi-filled symbols correspond to previous reports, the symbol a indicates *a*-out-of-plane orientation, and t indicates permeance of 0.5 μm thick MFI films grown on high flux supports. Dashed line represents the permeance of *n*-hexane through an α-Al_2O_3 disc. See Table 3 for details on the data used. Note: In the inset *n*-/*i*-butane separation factors from Tuan et al., 1999 and Tuan et al., 2000 are compared with *n*-Hexane/2,2-DMBseparation factors from Flanders et al., 2000 and Gade et al., 2001, respectively

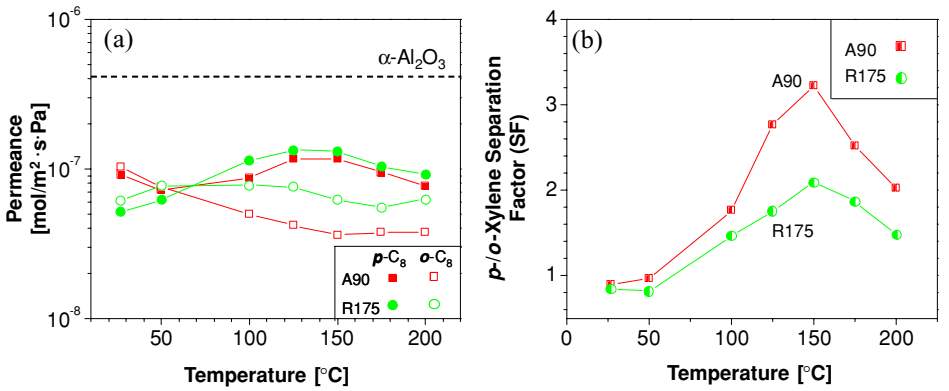

Fig. 10 (a) *p*-Xylene (*filled symbols*), *o*-xylene (*open symbols*) permeance and (b) *p*-/*o*-xylene separation factor (*semi-filled symbols*) vs. temperature for membranes A90 and R175. Dashed line represents the permeance of *p*-xylene through an α-Al_2O_3 disc

3.2.3 p-/o-Xylene

The separation performance microstructure relation discussed above does not extend beyond linear vs. branched hydrocarbon. It was demonstrated before that highly selective separation of xylene isomers (*p*-/*o*-xylene) can be accomplished using thin *b*-oriented MFI films, despite the fact that the selectivity of theses films for *n*-/*i*-butane is relatively low (Lai et al., 2003; Lai and Tsapatsis, 2004; Lai et al., 2004). Moreover, very small separation factors for xylene isomers (up to 3) are obtained from the thick columnar *c*-oriented films while

good separation performance can be obtained from thin *h0h*-oriented films (Xomeritakis et al., 2001). This contrast in *n*-/*i*-butane and *p*-/*o*-xylene separation performance is further confirmed by the current membranes. As shown in Fig. 10, membrane A90 has a higher separation factor for xylene isomers compared to membrane R175, while membrane R175 is more selective for linear vs. branched hydrocarbon (*n*-/*i*- butane and *n*-hexane/2,2-DMB) than membrane A90. This finding emphasizes the sensitivity of membrane performance on film microstructure and the importance of reproducibly controlling the latter. It also indicates that making performance predictions for certain mixtures like xylene isomers by extrapolation of performance in different separations is not a sound approach.

4 Conclusions

a- and randomly oriented seed layers were deposited by chemical bonding between support surface and zeolite seeds. The out-of-plane orientation is determined by the morphology of the seeds. The thin-along-a-axis anisometric seeds with the large basal *bc*-plane are deposited with an *a*-out-of-plane orientation, while the globular seeds are deposited as a random monolayer.

Secondary hydrothermal growth is applied to *a*- and randomly oriented seed layers. For *a*-oriented seed layers, the portion of *a*-out-of-plane orientation is reduced with time, while *h0h*- and *c*-oriented parts in films are gradually increased and finally become dominant. From randomly oriented seed layers, depending on the reaction temperature, preferentially *h0h*- and *c*-oriented columnar grains are obtained.

Permeation properties of MFI membranes made from an *a*-oriented seed layer are reported for the first time. Separation factors for *n*-/*i*-butane and *n*-hexane/2,2,-DMB are lower than those through columnar *c*- or *h0h*-oriented MFI films. A modest separation factor for *p*-/*o*-xylene was obtained. On the other hand, while the columnar films exhibit high *n*-/*i*-butane and the highest *n*-hexane/2,2-DMB separation factors, they show a smaller *p*-/*o*-xylene separation factor. Further studies are needed in order to decouple the effect of preferred orientation and other microstructure characteristics from thickness and intergrowth effects.

Acknowledgments Funding from NSF (CTS-0522518) and UOP LLC through IPrime is gratefully acknowledged. All characterizations were performed at the University of Minnesota Characterization Facility supported from NSF through the National Nanotechnology Infrastructure Network (NNIN).

References

Alfaro, S., M. Arruebo, J. Coronas, M. Menendez, and J. Santamaria, "Preparation of MFI Type Tubular Membranes by Steam-assisted Crystallization," *Microporous Mesoporous Mater.*, **50**(2–3), 195 (2001).

Arruebo, M., J.L. Falconer, and R.D. Noble, "Separation of Binary C5 and C6 Hydrocarbon Mixtures through MFI Zeolite Membranes," *J. Membr. Sci.*, **269**(1–2), 171 (2006).

Bernal, M.P., J. Coronas, M. Menendez, and J. Santamaria, "On the Effect of Morphological Features on the Properties of MFI Zeolite Membranes," *Microporous Mesoporous Mater.*, **60**(1–3), 99 (2003).

Bonilla, G., D.G. Vlachos, and M. Tsapatsis, "Simulations and Experiments on the Growth and Microstructure of Zeolite MFI Films and Membranes Made by Secondary Growth," *Microporous Mesoporous Mater.*, **42**(2–3), 191 (2001).

Bonilla, G., I. Diaz, M. Tsapatsis, H.-K. Jeong, Y. Lee, and D.G. Vlachos, "Zeolite (MFI) Crystal Morphology Control Using Organic Structure-Directing Agents," *Chem. Mater.*, **16**(26), 5697 (2004).

Bons, A.-J. and P.D. Bons, "The Development of Oblique Preferred Orientations in Zeolite Films and Membranes," *Microporous Mesoporous Mater.*, **62**(1–2), 9 (2003).

Caro, J., M. Noack, P. Kolsch, and R. Schafer, "Zeolite Membranes—State of their Development and Perspective," *Microporous Mesoporous Mater.*, **38**(1), 3 (2000).

Caro, J., M. Noack, and P. Koelsch, "Zeolite Membranes: From the Laboratory Scale to Technical Applications," *Adsorption*, **11**(3/4), 215 (2005).

Choi, J., S. Ghosh, Z. Lai, and M. Tsapatsis, "Uniformly a-Oriented MFI Zeolite Films by Secondary Growth," *Angew. Chem., Int. Ed.*, **45**(7), 1154 (2006).

Coronas, J., J.L. Falconer, and R.D. Noble, "Characterization and Permeation Properties of ZSM-5 Tubular Membranes," *AIChE J.*, **43**(7), 1797 (1997).

Coronas, J., R.D. Noble, and J. L. Falconer, "Separations of C4 and C6 Isomers in ZSM-5 Tubular Membranes," *Ind. Eng. Chem. Res.*, **37**(1), 166 (1998).

Coronas, J. and J. Santamaria, "State-of-the-Art in Zeolite Membrane Reactors," *Top. Catal.*, **29**(1–2), 29 (2004).

Davis, M.E., "Ordered Porous Materials for Emerging Applications," *Nature (London, U. K.)*, **417**(6891), 813 (2002).

Davis, T.M., T.O. Drews, H. Ramanan, C. He, J. Dong, H. Schnablegger, M.A. Katsoulakis, E. Kokkoli, A.V. McCormick, R.L. Penn, and M. Tsapatsis, "Mechanistic Principles of Nanoparticle Evolution to Zeolite Crystals," *Nature Materials*, **5**(5), 400 (2006).

de Vos Burchart, E., J.C. Jansen, B. van de Graaf, and H. van Bekkum, "Molecular Mechanics Studies on MFI-type Zeolites. Part 4. Energetics of Crystal Growth Directing Agents," *Zeolites*, **13**(3), 216 (1993).

Deckman, H.W., E.W. Corcoran, Jr., J.A. McHenry, W.F. Lai, L.R. Czarnetzki, and W.E. Wales, "Permselective Compositions Comprising a Substrate, a Zeolite or Zeolitelike Coating, and a Selectivity-enhancing Coating, and Separation and Catalytic Processes using the Compositions," WO 96/01686, (1996) [*Chem. Abstr.*, 1996, 124,180384p].

Flanders, C.L., V.A. Tuan, R.D. Noble, and J.L. Falconer, "Separation of C6 Isomers by Vapor Permeation and Pervaporation through ZSM-5 Membranes," *J. Membr. Sci.*, **176**(1), 43 (2000).

Funke, H.H., A.M. Argo, J.L. Falconer, and R.D. Noble, "Separations of Cyclic, Branched, and Linear Hydrocarbon Mixtures through Silicalite Membranes," *Ind. Eng. Chem. Res.*, **36**(1), 137 (1997).

Gade, S.K., V.A. Tuan, C.J. Gump, R.D. Noble, and J.L. Falconer, "Highly Selective Separation of *n*-hexane from Branched, Cyclic and Aromatic Hydrocarbons using B-ZSM-5 Membranes," *Chem. Commun.*, (7), 601–602 (2001).

Gora, L., J.C. Jansen, and T. Maschmeyer, "Controlling the Performance of Silicalite-1 Membranes," *Chem.–Eur. J.*, **6**(14), 2537 (2000).

Gora, L., N. Nishiyama, J.C. Jansen, F. Kapteijn, V. Teplyakov, and T. Maschmeyer, "Highly Reproducible High-flux Silicalite-1 Membranes: Optimization of Silicalite-1 Membrane Preparation," *Sep. Purif. Methods*, **22 and 23**(1–3), 223 (2001).

Gora, L. and J. C. Jansen, "Hydroisomerization of C6 with a Zeolite Membrane Reactor," *J. Catal.*, **230**(2), 269 (2005).

Gouzinis, A., and M. Tsapatsis, "On the Preferred Orientation and Microstructural Manipulation of Molecular Sieve Films Prepared by Secondary Growth," *Chem. Mater.*, **10**(9), 2497 (1998).

Gump, C.J., R.D. Noble, and J.L. Falconer, "Separation of Hexane Isomers through Nonzeolite Pores in ZSM-5 Zeolite Membranes," *Ind. Eng. Chem. Res.*, **38**(7), 2775 (1999).

Ha, K., Y.-J. Lee, H.J. Lee, and K.B. Yoon, "Facile Assembly of Zeolite monolayers on Glass, Silica, Alumina, and other Zeolites using 3-Halopropylsilyl Reagents as Covalent Linkers," *Adv. Mater. (Weinheim, Ger.)*, **12**(15), 1114 (2000).

Hedlund, J., J. Sterte, M. Anthonis, A.-J. Bons, B. Carstensen, N. Corcoran, D. Cox, H. Deckman, W. De Gijnst, P.-P. de Moor, F. Lai, J. McHenry, W. Mortier, J. Reinoso, and J. Peters, "High-flux MFI Membranes," *Microporous Mesoporous Mater.*, **52**(3), 179 (2002).

Hedlund, J., F. Jareman, A.-J. Bons, and M. Anthonis, "A Masking Technique for High Quality MFI Membranes," *J. Membr. Sci.*, **222**(1–2), 163 (2003).

Jareman, F., J. Hedlund, and J. Sterte, "Effects of Aluminum Content on the Separation Properties of MFI Membranes," *Sep. Purif. Methods*, **32**(1–3), 159 (2003).

Jeong, H.-K., Z. Lai, M. Tsapatsis, and J.C. Hanson, "Strain of MFI Crystals in Membranes. An in Situ Synchrotron x-ray Study," *Microporous and Mesoporous Materials*, **84**(1–3), 332 (2005).

Jiang, H., B. Zhang, Y.S. Lin, and Y. Li, "Synthesis of Zeolite Membranes," *Chin. Sci. Bull.*, **49**(24), 2547 (2004).

Kalipcilar, H., S.K. Gade, R.D. Noble, and J.L. Falconer, "Synthesis and Separation Properties of B-ZSM-5 Zeolite Membranes on Monolith Supports," *J. Membr. Sci.*, **210**(1), 113 (2002).

Keizer, K., A.J. Burggraaf, Z.A.E.P. Vroon, and H. Verweij, "Two Component Permeation through Thin Zeolite MFI Membranes," *J. Membr. Sci.*, **147**(2), 159 (1998).

Lai, Z., G. Bonilla, I. Diaz, J.G. Nery, K. Sujaoti, M.A. Amat, E. Kokkoli, O. Terasaki, R.W. Thompson, M. Tsapatsis, and D.G. Vlachos, "Microstructural Optimization of a Zeolite Membrane for Organic Vapor Separation," *Science (Washington, DC, U. S.)*, **300**(5618), 456 (2003).

Lai, Z. and M. Tsapatsis, "Gas and Organic Vapor Permeation through b-Oriented MFI Membranes," *Ind. Eng. Chem. Res.*, **43**(12), 3000 (2004).

Lai, Z., M. Tsapatsis, and J.P. Nicolich, "Siliceous ZSM-5 Membranes by Secondary Growth of b-oriented Seed Layers," *Adv. Funct. Mater.*, **14**(7), 716 (2004).

Lassinantti, M., F. Jareman, J. Hedlund, D. Creaser, and J. Sterte, "Preparation and Evaluation of thin ZSM-5 Membranes Synthesized in the Absence of Organic Template Molecules," *Catal. Today*, **67**(1–3), 109 (2001).

Lee, J.S., K. Ha, Y.-J. Lee, and K.B. Yoon, "Ultrasound-aided Remarkably Fast Assembly of Monolayers of Zeolite Crystals on Glass with a Very High Degree of Lateral Close Packing," *Adv. Mater. (Weinheim, Ger.)*, **17**(7), 837 (2005).

Li, G., E. Kikuchi, and M. Matsukata, "ZSM-5 Zeolite Membranes Prepared from a Clear Template-Free solution," *Microporous Mesoporous Mater.*, **60**(1–3), 225 (2003).

Li, Y., X. Zhang, and J. Wang, "Preparation for ZSM-5 Membranes by a Two-stage Varying-Temperature Synthesis," *Sep. Purif. Methods*, **25**(1–3), 459 (2001).

Lin, Y.S., I. Kumakiri, B.N. Nair, and H. Alsyouri, "Microporous Inorganic Membranes," *Sep. Purif. Methods*, **31**(2), 229 (2002).

Lovallo, M.C. and M. Tsapatsis, "Preferentially Oriented Submicron Silicalite Membranes," *AIChE J.*, **42**(11), 3020 (1996).

Lovallo, M.C., A. Gouzinis, and M. Tsapatsis, "Synthesis and Characterization of Oriented MFI Membranes Prepared by Secondary Growth," *AIChE J.*, **44**(8), 1903 (1998).

Lu, Y., R. Ganguli, C.A. Drewien, M.T. Anderson, C.J. Brinker, W. Gong, Y. Guo, H. Soyez, B. Dunn, M.H. Huang, and J.I. Zink, "Continuous Formation of Supported Cubic and Hexagonal Mesoporous Films by Sol-gel Dip-coating," *Nature (London, U. K.)*, **389**(6649), 364 (1997).

Mabande, G.T.P., S. Ghosh, Z. Lai, W. Schwieger, and M. Tsapatsis, "Preparation of b-oriented MFI Films on Porous Stainless Steel Substrates," *Ind. Eng. Chem. Res.*, **44**(24), 9086 (2005).

Matsufuji, T., N. Nishiyama, M. Matsukata, and K. Ueyama, "Separation of Butane and Xylene Isomers with MFI-type Zeolitic Membrane Synthesized by a Vapor-phase Transport Method," *J. Membr. Sci.*, **178**(1–2), 25 (2000a).

Matsufuji, T., N. Nishiyama, K. Ueyama, and M. Matsukata, "Permeation Characteristics of Butane Isomers through MFI-type Zeolitic Membranes," *Catal. Today*, **56**(1–3), 265 (2000b).

Matsufuji, T., K. Watanabe, N. Nishiyama, Y. Egashira, M. Matsukata, and K. Ueyama, "Permeation of Hexane Isomers through an MFI Membrane," *Ind. Eng. Chem. Res.*, **39**(7), 2434 (2000c).

McLeary, E.E. and J.C. Jansen, "Basic Views on the Preparation of Porous Ceramic Membrane Layers: A Comparison Between Amorphous and Crystalline Layers, Leading to a

New Method for the Preparation of Microporous Continuous Layers," *Top. Catal.*, **29**(1–2), 85 (2004).

McLeary, E.E., J.C. Jansen, and F. Kapteijn, "Zeolite Based Films, Membranes and Membrane Reactors: Progress and Prospects," *Microporous Mesoporous Mater.*, **90**(1–3), 198 (2006).

Meindersma, G.W. and A.B. de Haan, "Economical Feasibility of Zeolite Membranes for Industrial Scale Separations of Aromatic Hydrocarbons," *Desalination*, **149**(1–3), 29 (2002).

Nishiyama, N., L. Gora, V. Teplyakov, F. Kapteijn, and J.A. Moulijn, "Evaluation of Reproducible High Flux Silicalite-1 Membranes: Gas Permeation and Separation Characterization," *Sep. Purif. Technol.*, **22 and 23**(1–3), 295 (2001).

Noack, M., P. Kolsch, R. Schafer, P. Toussaint, and J. Caro, "Molecular Sieve Membranes for Industrial Application: Problems, Progress, Solutions," *Chem. Eng. Technol.*, **25**(3), 221 (2002).

Piera, E., M.P. Bernal, M.A. Salomon, J. Coronas, M. Menendez, and J. Santamaria, "Preparation and Permeation Properties of Different Zeolite Tubular Membranes," *Stud. Surf. Sci. Catal.*, **125**(Porous Materials in Environmentally Friendly Processes), 189 (1999).

Tuan, V.A., J.L. Falconer, and R.D. Noble, "Alkali-Free ZSM-5 Membranes: Preparation Conditions and Separation Performance," *Ind. Eng. Chem. Res.*, **38**(10), 3635 (1999).

Tuan, V.A., R.D. Noble, and J.L. Falconer, "Boron-substituted ZSM-5 Membranes: Preparation and Separation Performance," *AIChE J.*, **46**(6), 1201 (2000).

van de Graaf, J.M., E. van der Bijl, A. Stol, F. Kapteijn, and J.A. Moulijn, "Effect of Operating Conditions and Membrane Quality on the Separation Performance of Composite Silicalite-1 Membranes," *Ind. Eng. Chem. Res.*, **37**(10), 4071 (1998).

Verduijn, J.P., A.-J. Bons, M.H.C. Anthonis, and L.R. Czarnetzki, "Structures Comprising a Support, an Intermediate Layer, and an Upper Layer, Process for Forming a Molecular Sieve Layer on Supports, the Products Obtained, and Process for Separating Fluid Mixtures and Catalyzing Chemical Reactions with the Resulting Zeolite Membranes," WO 96/01683, (1996) [*Chem. Abstr.*, 1996, 124:236420s].

Vroon, Z.A.E.P., K. Keizer, M.J. Gilde, H. Verweij, and A.J. Burggraaf, "Transport Properties of Alkanes through Ceramic Thin Zeolite MFI Membranes," *J. Membr. Sci.*, **113**(2), 293 (1996).

Vroon, Z.A.E.P., K. Keizer, A.J. Burggraaf, and H. Verweij, "Preparation and Characterization of Thin Zeolite MFI Membranes on Porous Supports," *J. Membr. Sci.*, **144**(1–2), 65 (1998).

Xomeritakis, G., A. Gouzinis, S. Nair, T. Okubo, M. He, R.M. Overney, and M. Tsapatsis, "Growth, Microstructure, and Permeation Properties of Supported Zeolite (MFI) Films and Membranes Prepared by Secondary Growth," *Chem. Eng. Sci.*, **54**(15–16), 3521 (1999).

Xomeritakis, G., S. Nair, and M. Tsapatsis, "Transport Properties of Alumina-supported MFI Membranes Made by Secondary (Seeded) Growth," *Microporous Mesoporous Mater.*, **38**(1), 61 (2000).

Xomeritakis, G., Z. Lai, and M. Tsapatsis, "Separation of Xylene Isomer Vapors with Oriented MFI Membranes Made by Seeded Growth," *Ind. Eng. Chem. Res.*, **40**(2), 544 (2001).